AJNR

MR Imaging Characteristics and ADC Histogram Metrics for Differentiating Molecular Subgroups of Pediatric Low-Grade Gliomas

S. Shrot, A. Kerpel, J. Belenky, M. Lurye, C. Hoffmann and M. Yalon

AJNR Am J Neuroradiol 2022, 43 (9) 1356-1362
doi: https://doi.org/10.3174/ajnr.A7614
http://www.ajnr.org/content/43/9/1356

MR Imaging Characteristics and ADC Histogram Metrics for Differentiating Molecular Subgroups of Pediatric Low-Grade Gliomas

S. Shrot, A. Kerpel, J. Belenky, M. Lurye, C. Hoffmann, and M. Yalon

ABSTRACT

BACKGROUND AND PURPOSE: *BRAF* and type 1 neurofibromatosis status are distinctive features in pediatric low-grade gliomas with prognostic and therapeutic implications. We hypothesized that DWI metrics obtained through volumetric ADC histogram analyses of pediatric low-grade gliomas at baseline would enable early detection of *BRAF* and type 1 neurofibromatosis status.

MATERIALS AND METHODS: We retrospectively evaluated 40 pediatric patients with histologically proved pilocytic astrocytoma ($n = 33$), ganglioglioma ($n = 4$), pleomorphic xanthoastrocytoma ($n = 2$), and diffuse astrocytoma grade 2 ($n = 1$). Apart from 1 patient with type 1 neurofibromatosis who had a biopsy, 11 patients with type 1 neurofibromatosis underwent conventional MR imaging to diagnose a low-grade tumor without a biopsy. *BRAF* molecular analysis was performed for patients without type 1 neurofibromatosis. Eleven patients presented with *BRAF* V600E-mutant, 20 had *BRAF-KIAA* rearrangement, and 8 had *BRAF* wild-type tumors. Imaging studies were reviewed for location, margins, hemorrhage or calcifications, cystic components, and contrast enhancement. Histogram analysis of tumoral diffusivity was performed.

RESULTS: Diffusion histogram metrics (mean, median, and 10th and 90th percentiles) but not kurtosis or skewness were different among pediatric low-grade glioma subgroups ($P < .05$). Diffusivity was lowest in *BRAF* V600E-mutant tumors (the 10th percentile reached an area under the curve of 0.9 on receiver operating characteristic analysis). There were significant differences between evaluated pediatric low-grade glioma margins and cystic components ($P = .03$ and $P = .001$, respectively). Well-defined margins were characteristic of *BRAF-KIAA* or wild-type *BRAF* rather than *BRAF* V600E-mutant or type 1 neurofibromatosis tumors. None of the type 1 neurofibromatosis tumors showed a cystic component.

CONCLUSIONS: Imaging features of pediatric low-grade gliomas, including quantitative diffusion metrics, may assist in predicting *BRAF* and type 1 neurofibromatosis status, suggesting a radiologic-genetic correlation, and might enable early genetic signature characterization.

ABBREVIATIONS: AUC = area under the curve; GG = ganglioglioma; MAPK = mitogen-activated protein kinase pathway; NF1 = type 1 neurofibromatosis; pLGG = pediatric low-grade glioma; rADC = relative ADC; RAS = rat sarcoma virus; ROC = receiver operating characteristic

Pediatric low-grade gliomas (pLGGs) are the most frequent brain tumors in children.[1] pLGGs are defined as World Health Organization grade I or II malignancies and include a wide array of histologies, such as juvenile pilocytic astrocytoma, ganglioglioma (GG), dysembryoplastic neuroepithelial tumor, and pleomorphic xanthoastrocytoma.[2] The components of treatment for pLGGs have historically been surgery, radiation, and multiagent chemotherapy. Surgical resection may be curative in the case of gross total resection. However, most children cannot undergo complete resection due to the location of the tumor. Ten-year progression-free survival drops significantly if a radiologically visible residual tumor is evident.[3] In such patients, adjuvant focal radiation therapy was performed in the past. However, due to the long-term adverse effects of radiation, adjuvant chemotherapy has been the main treatment technique for patients with pLGG.

BRAF is a serine/threonine-protein kinase that has a key role in growth signal transduction. In the past decade, emerging molecular data have suggested that in pLGGs, there is near-universal up-regulation of the rat sarcoma virus (RAS)-mitogen-activated protein kinase pathway (MAPK),[4] most commonly due to somatic alterations involving the *BRAF* proto-oncogene or germline type 1

Received February 28, 2022; accepted after revision June 28.

From the Section of Neuroradiology, Division of Diagnostic Imaging (S.S., A.K., J.B., C.H.) and Department of Pediatric Hemato-Oncology (M.L., M.Y.), Sheba Medical Center, Ramat-Gan, Israel; and Sackler School of Medicine (S.S., C.H., M.Y.), Tel Aviv University, Tel Aviv, Israel.

Please address correspondence to Shai Shrot, MD, Section of Neuroradiology, Division of Diagnostic Imaging, Sheba Medical Center, 2 Sheba Rd, Ramat Gan, 52621 Israel; e-mail: shai.shrot@sheba.health.gov.il

Indicates article with online supplemental data.

http://dx.doi.org/10.3174/ajnr.A7614

neurofibromatosis (NF1) alterations.[5] The 2 major *BRAF* gene alterations in pLGG are *BRAF* rearrangement (duplication of the *BRAF* oncogene, followed by its insertion into 1 of several fusion targets, most often the *KIAA1549* gene) and *BRAF* V600E point mutation (V600E).[4] These molecular alterations in the *BRAF* gene lead to constitutive activation of the kinase and downstream signaling pathways that drive uncontrolled cell proliferation and tumorigenesis.

NF1 is a common autosomal dominant disorder that results in the most frequent tumor predisposition syndrome. Neurofibromin, the protein product of the *NF1* gene that is mutated in patients with NF1, has been shown to function as a tumor-suppressor gene, acting as a negative regulator of RAS. Loss of neurofibromin increases RAS activity and induces downstream activity of the MAPK pathway as well as the PI3K-Akt-mammalian target of rapamycin (mTOR) pathway.[5] Approximately 15% of children with NF1 develop low-grade optic pathway gliomas. Therefore, optic pathway gliomas in these patients are primarily diagnosed via germline *NF1* alteration and imaging rather than a biopsy.[6]

Exploring the *BRAF* status of pLGGs improves risk-stratification and tailored targeted therapies in patients with residual disease in whom additional therapy is needed.[7] Whereas patients with *BRAF* fusion and NF1 have a favorable outcome, those with the *BRAF* V600E mutation, particularly associated with cyclin-dependent kinase inhibitor 2A (CDNK2A) deletion, are at increased risk of progression with shorter progression-free survival rates and worse response to chemotherapy.[7,8] Furthermore, molecularly targeted therapies have been shown to be effective in patients with residual pLGGs; for instance, type I *BRAF* inhibitors for *BRAF* V600E pLGG and mitogen-activated protein kinase inhibitors for pLGGs driven by *NF1*, *BRAF-KIAA* rearrangement, or *BRAF* V600E mutation. Most important, type I *BRAF* inhibitors have been shown to result in paradoxical activation and accelerating growth of pLGGs driven by the *BRAF-KIAA* fusion.[9] Therefore, identifying the exact molecular alteration is crucial.

Radiogenomic techniques, which have emerged as valuable imaging tools to characterize brain tumors noninvasively, have a pivotal role in making treatment decisions in patients with pLGGs. Recently, a few studies have described imaging features of pLGGs in correlation with their *BRAF* status.[10,11] Ramaglia et al[11] found lower ADC values in V600E-mutant pLGGs, though no morphologic imaging characteristics were found to have discriminative power from wild-type *BRAF*. More advanced ADC metrics (such as histogram analysis) found to be of diagnostic value in pediatric tumors[12,13] have not been evaluated in the genetic characterization of pLGG (*BRAF* or *NF1* status). We hypothesized that ADC metrics obtained through volumetric ADC histogram analyses of pLGGs at baseline would enable early detection of *BRAF* and *NF1* status.

MATERIALS AND METHODS

The institutional review board of the Sheba Medical Center approved this retrospective study.

Study Design and Population

Patients with pLGG, diagnosed and treated in our tertiary pediatric neuro-oncology clinics, were included. Inclusion criteria were the following: 1) available baseline presurgical MR imaging, and 2) biopsy and characteristics of *BRAF* status or a diagnosis of germling *NF1*. Exclusion criteria included a markedly degraded MR imaging study, pure optic nerve involvement, and spinal location.

Brain MR Imaging

MR imaging studies were performed in multiple centers on 1.5T or 3T magnets across various vendors. All patients had routine clinical MR imaging scans, including precontrast and postcontrast T1-weighted images, T2-FLAIR, and T2-weighted images. These sequences were performed with variable section thickness ranging from 1 to 5 mm. Heme-sensitive sequences, such as T2* gradient recalled-echo or SWI, were available in 33 patients. On each scanner, the DWI acquisition consisted of a diffusion-sensitized axial 2D spin-echo sequence with an EPI readout, with 2 *b* values of 0 and 1000 s/mm^2. Section thickness ranged from 3 to 4 mm, with interslice gaps of 0–1 mm.

Image Analysis

We analyzed the following tumoral morphologic imaging features: the presence of well-defined margins, a cystic component, contrast enhancement, and hemorrhagic components or calcifications, which were evaluated only in cases with available heme-sensitive MR imaging sequences (T2* or SWI) or CT scans. These were recorded as binary variables. As for location, classification was according to the epicenter of the tumor (cerebral hemispheres, cerebellum, brainstem, or diencephalon). All images were assessed in consensus by 2 board-certified neuroradiologists (J.B. and S.S.) with 3 and 6 years of experience, respectively, blinded to the pathologic diagnosis.

DWI Measurements

Tumor segmentation was performed by a board-certified radiologist (A.K.) and was confirmed in consensus by a board-certified neuroradiologist with 6 years of neuroradiology experience (S.S.) using 3D Slicer (Version 4.11.2; http://www.slicer.org[14]). Semiautomated tumor segmentation was performed on T2-FLAIR images in all respective MR imaging sections on noncystic, noncalcified, or hemorrhagic tumor areas using the level tracing effect tool. All ROIs were then copied to the automatically coregistered corresponding ADC maps via 3D Slicer. The transposed volumetric ROI was evaluated and manually corrected on the ADC maps, if necessary, by A.K. and S.S. in consensus. DWI metrics and histogram analysis of the selected volumetric whole-lesion ROIs were performed using the module SlicerRadiomics extension.[15] For normalization of ADC values, a circular ROI was drawn on the right eye and left thalamus. Relative ADC (rADC) ratios were calculated by dividing each ADC metric of the lesion by the mean ADC value of the right eye and the normal-appearing thalamus. This step was performed to adjust ADC values across MR imaging vendors and magnetic field strengths.

Statistical Analysis

Descriptive statistics included mean and SD of continuous parameters; in the case of categoric factors, number and percentage distribution were used. The χ^2 test was used to analyze the differences in the categoric parameters and qualitative features among the various molecular tumor groups. DWI histogram analysis included

10th and 90th percentiles, mean, median, skewness, and kurtosis. The Kruskal-Wallis test with the post hoc Dunn-Bonferroni method was used to compare diffusivity metrics among genetic subgroups. *P* values have been adjusted by the Bonferroni correction for multiple comparisons. Receiver operating characteristic (ROC) curve analysis was performed, and the respective area under the curve (AUC) was calculated to assess the accuracy of ADC histogram features in differentiating various pLGG subgroups. The ROC curve plots the true-positive rate against the false-positive rate at various threshold settings. The DeLong test was used for the comparison of various AUCs. A 2-tailed $P < .05$ was considered statistically significant. Analyses were performed with SPSS (Version 27.0, 2021; IBM).

RESULTS

Study Population

The study cohort (Fig 1) included 51 patients in whom histologically proved tumors included pilocytic astrocytoma ($n = 33$), GG ($n = 4$), pleomorphic xanthoastrocytoma ($n = 2$), and diffuse astrocytoma grade II ($n = 1$). Of patients with NF1, 11 underwent imaging with a diagnosis of a low-grade tumor without a biopsy.

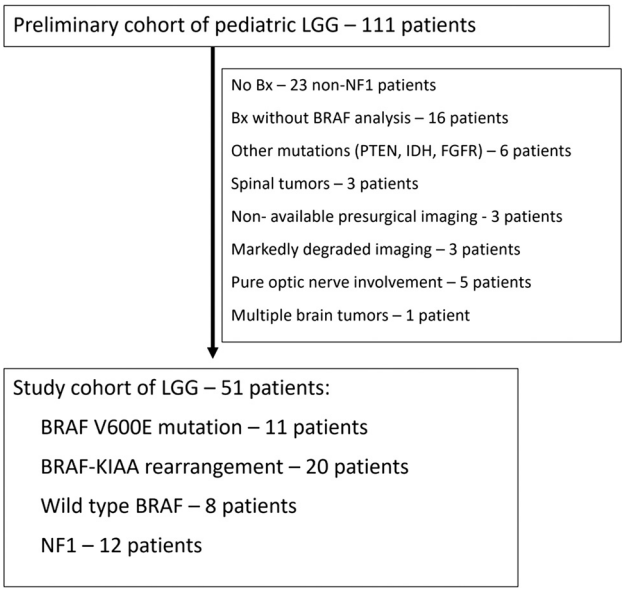

FIG 1. Study flow chart. Bx indicates biopsy.

One patient with NF1 underwent a biopsy with a histology of GG. *BRAF* molecular analysis was performed for patients without NF1. Eleven patients presented with the *BRAF* V600E mutation; 20 patients had *BRAF-KIAA* rearrangement, and 8 had *BRAF* wild-type tumors. pLGG was diagnosed at a younger age in patients with *BRAF-KIAA* rearrangement and NF1 groups than in *BRAF* V600E-mutant or wild-type *BRAF* groups ($P = .03$). The major demographic data are presented in Table 1.

Morphologic MR Imaging Findings

Ill-defined borders were more characteristic of *BRAF* V600E-mutant tumors rather than in *BRAF-KIAA* rearrangement or wild-type *BRAF* pLGGs. Examples of MR images of pLGGs are shown in Fig 2. Hemorrhagic components or calcifications were seen in wild-type *BRAF* tumors compared with *BRAF* alterations of NF1 tumors. Lack of a cystic component characterized NF1 tumors compared with *BRAF* alteration of wild-type *BRAF* tumors. No significant differences were found among study groups in terms of tumor location. A summary of the morphological imaging findings is presented in Table 2.

Diffusion Metrics

Significant differences were found in evaluated diffusion metrics between pLGG subgroups, except for kurtosis and skewness (Online Supplemental Data). These results were similar when ADC measurements were normalized to the thalamus or the eye globe. For most diffusivity metrics, rADC measurements were lower in *BRAF* V600E-mutant tumors than in the *BRAF-KIAA* rearrangement subgroup (representative metrics are presented in Fig 3). $rADC_{mean}$ and $rADC_{median}$ (relative to the thalamus) were significantly lower in NF1 tumors compared with *BRAF-KIAA* rearrangement or wild-type *BRAF* subgroups ($P < .001$). Differences in diffusion histogram metrics among pLGG subgroups were also significant when excluding NF1 tumors (Online Supplemental Data).

According to ROC curve analyses, the $rADC_{10}$ values had the highest AUC values for differentiating *BRAF* V600E-mutant from the *BRAF-KIAA* rearrangement group (AUC = 0.895 and 0.905, relative to the thalamus or eye globe, respectively). $rADC_{10}$ values also had high diagnostic performances for differentiating *BRAF* V600E-mutant from *BRAF-KIAA* rearrangement or wild-type *BRAF* (AUC = 0.873 and 0.864, relative to the thalamus or eye globe, respectively). However, the high performance of $rADC_{10}$ did not reach statistical significance compared with other diffusivity metrics. For differentiating NF1 tumors from wild-

Table 1: Major clinical characteristics and tumor histology in various pLGG subgroups

	BRAF V600E-Mut ($n = 11$)	*BRAF-KIAA* Rearrangement ($n = 20$)	Wild-Type *BRAF* ($n = 8$)	NF1 ($n = 12$)	*P* Value
Sex (male/female)	8/3	7/13	5/3	7/5	.45
Age at diagnosis (mean) (yr)	9.1 (SD, 4.7)	5.4 (SD, 3.9)	14.6 (SD, 8.7)	4.9 (SD, 2.9)	.03
Histology (No.)					
PA	7	19	7		
GG	2		1	1[a]	
PXA	2				
Diffuse astrocytoma (grade II)		1			

Note:—PA indicates pilocytic astrocytoma; PXA, pleomorphic xanthoastrocytoma; Mut, mutant.
[a] In 1 patient with NF1, a ganglioglioma was found at biopsy.

type or altered *BRAF*, the performance of diffusivity metrics was relatively low, except for $rADC_{min}$ (AUC = 0.803 and 0.746, relative to the thalamus or eye globe, respectively). Overall, diagnostic performances were similar when comparing the normalization of ADC values with that of the thalamus or eye globe. In NF1 tumors, except for $rADC_{min}$, there was higher discriminative power for normalization to the globe over the thalamus ($P < .001–.02$), even though absolute AUC values were relatively low. The diagnostic performance of $rADC_{min}$, $rADC_{10}$, $rADC_{90}$, $rADC_{mean}$, and $rADC_{median}$ for differentiating various pLGG subgroups is summarized in the Online Supplemental Data.

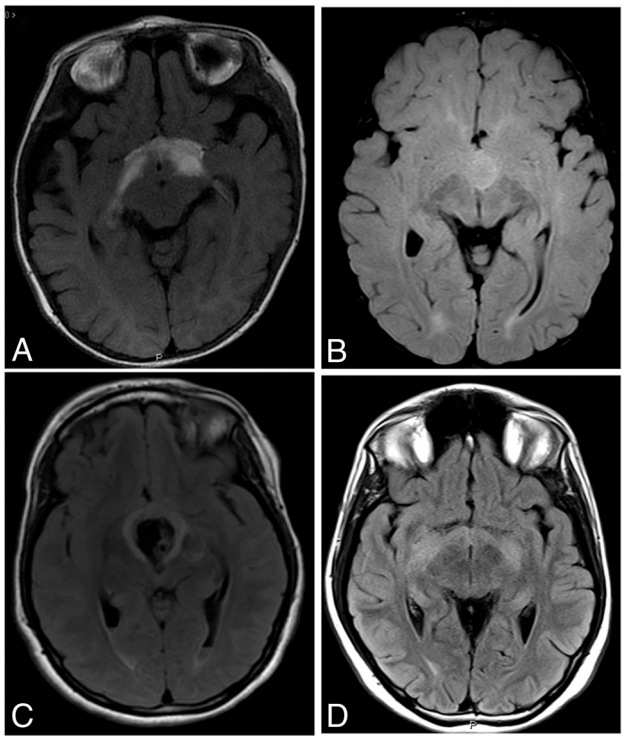

FIG 2. Representative T2-FLAIR images of pLGGs of various molecular subgroups. *A*, A 5-month-old boy with a diencephalic pLGG infiltrating the optic tracts (*BRAF*-mutant). *B*, A 15-year-old boy with a well-defined diencephalic pLGG (*BRAF-KIAA* rearrangement), *C*, A 20-year-old woman with well-defined diencephalic pLGG (wild-type *BRAF*), associated with a large central hemorrhagic area. *D*, A 16-year-old boy with a typical diencephalic glioma infiltrating the optic tracts (NF1).

DISCUSSION

In the past decade, there has been increasing evidence of the importance of *BRAF* status, which has major therapeutic and prognostic implications in pLGGs, especially if these tumors are unresectable.[7] Currently, most non-NF1 pLGGs undergo surgical biopsy for genetic analysis, even if curative resection is not possible. Our results suggest that in pLGGs, morphologic MR imaging features show significant differences according to *BRAF* and *NF1* status, which might improve the early prediction of the genetic alterations of pLGGs. Quantitative diffusion metrics from cumulative ADC histograms based on the T2-FLAIR imaging abnormalities were found to be promising for differentiating pLGG subgroups. However, other parameters of histogram distribution, particularly kurtosis and skewness, have limited diagnostic value.

The ill-defined border of the pLGG, radiographically suggesting infiltration, was found in our cohort to be more characteristic for *BRAF* V600E-mutant pLGGs (10/11) compared with wild-type *BRAF* (5/13) or *BRAF-KIAA* rearrangement (11/20). Ho et al[10] have described peritumoral T2 abnormality, suggesting infiltration in half the *BRAF* V600E-mutant pLGGs compared with a minority (~8%) of wild-type *BRAF* tumors. Most interesting, such infiltration is a well-known feature of NF1 tumors, also found in our cohort (10/12). In our cohort, hemorrhagic components or calcifications were characteristic of wild-type *BRAF* pLGG over other *BRAF* alterations or NF1 tumors.

Nevertheless, there is usually an overlap of qualitative imaging characteristics, limiting their use in defining the pLGG subgroup signature. Studies describing quantitative imaging features differentiating pLGG molecular subgroups are even more sparse than

Table 2: Morphologic MR imaging characteristics

	BRAF V600E-Mut ($n = 11$)	*BRAF-KIAA* Rearrangement ($n = 20$)	Wild-Type *BRAF* ($n = 8$)	NF1 ($n = 12$)	*P* Value
Location (No.) (%)					
Cerebral hemisphere	3 (27.3%)	3 (15%)	1 (12.5%)	1 (8.3%)	.15
Cerebellum	1 (9.1%)	7 (35%)	5 (62.5%)	2 (16.7%)	
Brainstem	2 (18.2%)	6 (30%)	0 (0%)	2 (16.7%)	
Diencephalon	5 (45.5%)	4 (20%)	2 (25%)	7 (58.3%)	
Well-defined margins (yes/no)	9.1% (1/10)	45.0% (9/11)	62.5% (5/3)	16.6% (2/10)	.03[a,b,c]
Hemorrhagic components or calcifications (yes/no)*	0% (0/8)	15.3% (2/11)	62.5% (5/3)	0% (0/6)	.005[b,c,f]
Cystic components (yes/no)	45.4% (5/6)	60% (12/8)	87.5% (7/1)	0% (0/12)	.001[c,d,e]
Contrast enhancement (yes/no)	81.8% (9/2)	85% (17/3)	100% (8/0)	50% (6/6)	.04[c,d]

Note:—Mut indicates mutant. Each superscript letter represents a significant difference between 2 categories.
[a] *BRAF* V600E-mutant versus *BRAF-KIAA* rearrangement.
[b] *BRAF* V600E-mutant versus *BRAF* wild-type.
[c] *BRAF* wild-type versus NF1.
[d] *BRAF* V600E-mutant versus NF1.
[e] *BRAF-KIAA* rearrangement versus NF1.
[f] *BRAF* wild-type versus *BRAF-KIAA* rearrangement.
* Evaluated only when SWI/T2* or CT scans were available ($n = 35$).

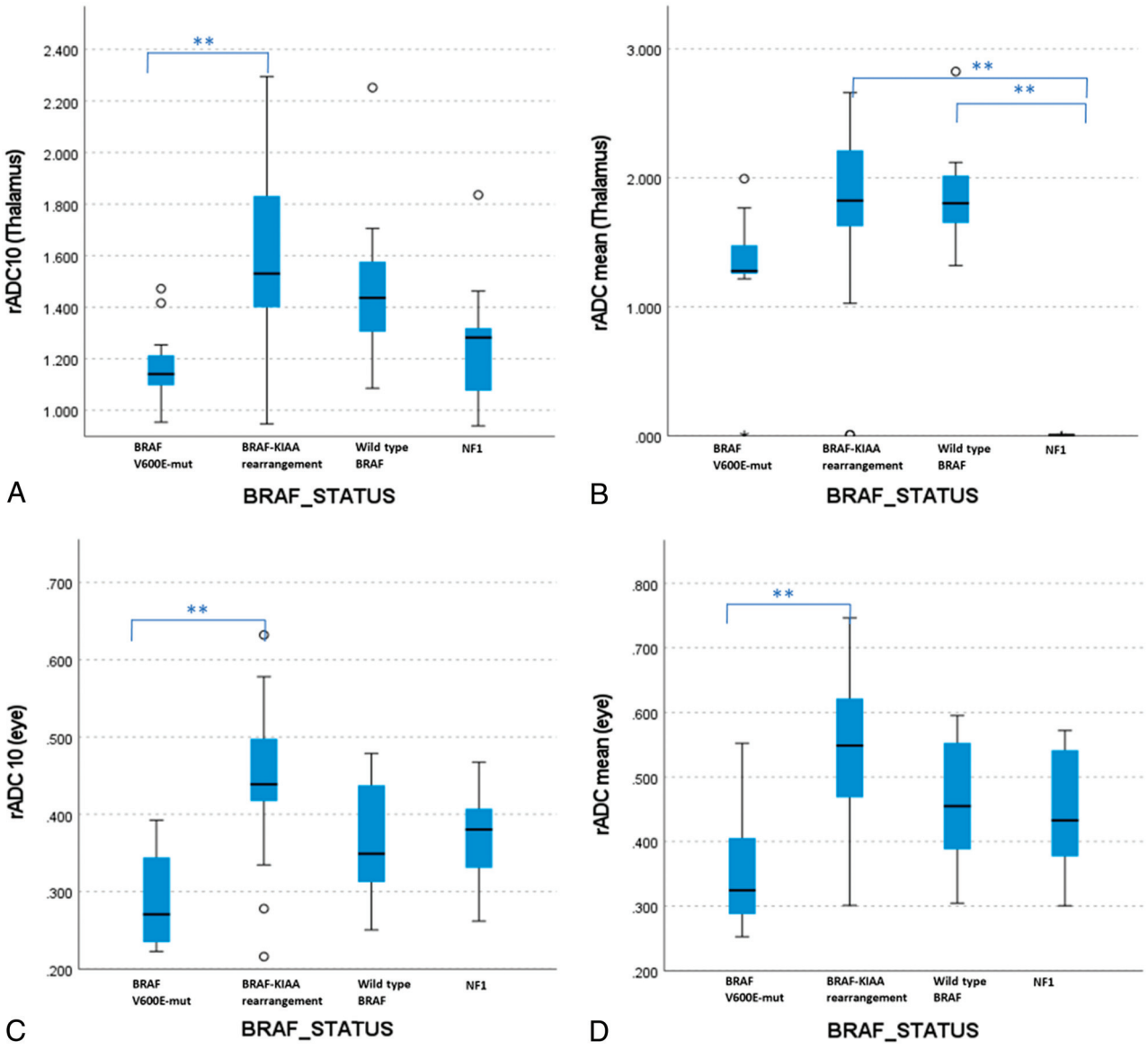

FIG 3. Boxplots comparing $rADC_{10}$ and $rADC_{mean}$, relative to the mean ADC values of the right thalamus (*A* and *B*, respectively) or the right eye globe (*C* and *D*, respectively). Group differences were significant ($P < .001$, Kruskal-Wallis test). Significant pair-wise differences are indicated in the figure (Dunn-Bonferroni post hoc analysis, *Double asterisks* indicate $P < .005$).

descriptive imaging studies. To our knowledge, there have been only a limited number of reports regarding genetic profiling of pLGG using DWI and no literature reports investigating the usefulness of the ADC histogram for such analysis. In our study, *BRAF* V600E-mutant pLGGs showed decreased diffusivity on various diffusion histogram metrics (ADC_{10}, ADC_{90}, mean and median ADC values) compared with *BRAF-KIAA* rearrangement pLGGs. Similar results were also reported by Ramaglia et al[11] for *BRAF* V600E-mutant pLGG, compared with wild-type *BRAF*, though *BRAF-KIAA* rearrangement or NF1 pLGG were not included in their study.

In a small case series, Ishi et al[16] described a lower T2 signal and a larger T2/contrast-enhanced T1 mismatch to be more suggestive of *BRAF* V600E-mutation in optic pathway gliomas. Recently, Wagner et al described using a machine learning scheme to differentiate pLGG genetics subgroups according to their T2-FLAIR features.[17] Although machine learning–based approaches might detect differences in neuroimaging data that might not be identified with conventional approaches, such as multiple T2-FLAIR features, traditional statistical approaches, such as used in the current study, might improve our understanding of the different radiologic-pathologic correlations in various pLGGs. Although isocitrate dehydrogenase (*IDH*) mutations are rare among pLGGs,[18] diffusion metrics were also found to assist in differentiating *IDH* status in adult LGGs.[19,20] Most ADC percentiles were found to be lower in *IDH*-negative compared with *IDH*-mutated gliomas.

DWI reflects the free motion of water molecules in biologic tissue.[21] Highly cellular tumors, ie, with a high nuclear-to-cytoplasmic ratio, typically show diffusion restriction with decreased ADC values.[22] Ho et al[10] have described a distinctive histologic pattern in *BRAF* V600E-mutant pLGG of a monophasic dense, compact architecture resembling the compact, fiber-rich regions previously described in pilocytic astrocytomas, which might explain the

decreased diffusivity found in these tumors in our cohort compared with wild-type *BRAF* pLGG. For ADC measurements, most studies used ROI analysis to evaluate brain lesions. Such analysis is based on the representative part of the lesion.[23,24] However, selecting a representative location is subjective and may be difficult, especially when the lesion is heterogeneous and includes atypical imaging features. ADC histogram analysis was found to be useful for grading gliomas and predicting the treatment response and progression-free survival rates in patients with high-grade gliomas.[25-27] Given that histogram analysis includes an entire lesion, it may reveal the heterogeneity of lesions and thus ensure more accurate tissue characteristics.

NF1 is a tumor-predisposition genetic disorder, usually diagnosed using a clinical phenotype indicative of a germline *NF1* mutation.[6] The most common CNS tumors in NF1 are low-grade gliomas, with the optic pathway glioma being the hallmark lesion. Surgery is not the first treatment choice in NF1-associated gliomas, which are commonly nonresectable and have a relatively benign course. However, infiltrative optic pathway pLGG, typical of patients with NF1, might have a *BRAF* alteration rather than an *NF1* mutation, a difference that has major clinical consequences.[28] A biopsy is often performed in such cases, especially if NF1 cannot be diagnosed clinically or genetically. Our results might also assist in identifying the imaging signature of NF1 pLGG relative to other *BRAF*-altered gliomas.

The reproducibility of lesional ADC measurements over various field strengths, different vendors, and acquisition parameters is critical for the applicability of our results. Multiple in vivo studies have reported near-identical ADC measurements on 1.5T and 3T scanners.[29,30] However, other phantoms and in vivo studies have demonstrated a significant ADC difference among different magnet fields.[31,32] Therefore, Sasaki et al[31] have suggested using rADC values because they might be more suitable than absolute ADC values for evaluating diffusion abnormalities acquired in different scanners and field strengths. ROIs drawn on the normal-appearing white matter[33] or gray matter[11] are commonly used for ADC normalization. We have calculated the rADC values normalized to the normal-appearing thalamus and the eye globe to minimize the differences among absolute ADC values across various platforms. Both references have shown similar reproducible and discriminative results among various pLGG subgroups. Such rADCs are robust across MR imaging vendors and platforms and may be considered reliable.[11,34] The ADC histogram analysis technique used in the current study is a promising method that can be used on clinically acquired diffusion MR imaging data for subsequent analysis, allowing comparison at different institutions and use in multicenter clinical trials.

There are several limitations to our study. First, our study was a retrospective investigation of a relatively small patient cohort. More pLGGs will be required to strengthen the statistical power and generalize our results in future studies. Due to the small cohort, obtaining ADC thresholds from ROC-AUC, which can be used in clinical settings, is limited. Second, accurately defining the imaging borders of infiltrative lesions is suboptimal, with relatively high interobserver variability. Given the large volumetric data included in the histogram analysis of an entire lesion, the nonperfect delineation of the lesion boundaries is relatively acceptable compared with ROI analysis. Last, tumor delineation was performed on T2-FLAIR images, and coregistration of T2-FLAIR imaging with the ADC map was required in our study. Although the tumor was carefully delineated, there is still the possibility of misregistration and the inclusion of erroneous ADC values at the tumor boundaries.

In the current study, diffusion metrics have improved radiologic-genetic correlation in pLGGs. Such tumoral quantitative features have the potential for better characterizing tumor structure and evaluating early treatment-related changes. Diffusion metrics have been shown to correlate and even predict the response to radiation or biologic treatment in high-grade gliomas.[35,36] Moreover, Poussaint et al[37] described a significant correlation between diffusion metrics and survival in patients with diffuse intrinsic pontine gliomas. In the current study, due to the small number of patients and heterogenicity of treatment protocols, such correlation between diffusion metrics and response to treatment could not be assessed.

CONCLUSIONS

Our results suggest that ADC histogram analysis based on an entire pLGG could help to discriminate various pLGG genetic subgroups, thus expanding and refining the correlation between clinically acquired imaging, including DWI, and the pLGG genetic signature. Such radiologic-genetic correlation has a critical role in the early detection of molecular subgroups and early clinical stratification of children with pLGGs.

Disclosure forms provided by the authors are available with the full text and PDF of this article at www.ajnr.org.

REFERENCES

1. Ostrom QT, de Blank PM, Kruchko C, et al. **Alex's Lemonade Stand Foundation Infant and Childhood Primary Brain and Central Nervous System Tumors Diagnosed in the United States in 2007-2011.** *Neuro Oncol* 2015;16(Suppl 10):x1–36 CrossRef Medline
2. Komori T. **The 2016 WHO Classification of Tumours of the Central Nervous System: the major points of revision.** *Neurol Med Chir (Tokyo)* 2017;57:301–11 CrossRef Medline
3. Wisoff JH, Sanford RA, Heier LA, et al. **Primary neurosurgery for pediatric low-grade gliomas: a prospective multi-institutional study from the Children's Oncology Group.** *Neurosurgery* 2011;68:1548–54; discussion 1554–55 CrossRef Medline
4. AlRayahi J, Zapotocky M, Ramaswamy V, et al. **Pediatric brain tumor genetics: what radiologists need to know.** *Radiographics* 2018;38:2102–22 CrossRef Medline
5. Szudek J, Birch P, Riccardi VM, et al. **Associations of clinical features in neurofibromatosis 1 (NF1).** *Genet Epidemiol* 2000;19:429–39 CrossRef Medline
6. Helfferich J, Nijmeijer R, Brouwer OF, et al. **Neurofibromatosis type 1 associated low grade gliomas: a comparison with sporadic low grade gliomas.** *Crit Rev Oncol Hematol* 2016;104:30–41 CrossRef Medline
7. Vuong HG, Altibi AM, Duong UN, et al. **BRAF mutation is associated with an improved survival in glioma-a systematic review and meta-analysis.** *Mol Neurobiol* 2018;55:3718–24 CrossRef Medline
8. Mistry M, Zhukova N, Merico D, et al. **BRAF mutation and CDKN2A deletion define a clinically distinct subgroup of childhood secondary high-grade glioma.** *J Clin Oncol* 2015;33:1015–22 CrossRef Medline

9. Karajannis MA, Legault G, Fisher MJ, et al. **Phase II study of sorafenib in children with recurrent or progressive low-grade astrocytomas.** *Neuro Oncol* 2014;16:1408–16 CrossRef Medline
10. Ho CY, Mobley BC, Gordish-Dressman H, et al. **A clinicopathologic study of diencephalic pediatric low-grade gliomas with BRAF V600 mutation.** *Acta Neuropathol* 2015;130:575–85 CrossRef Medline
11. Ramaglia A, Tortora D, Mankad K, et al. **Role of diffusion weighted imaging for differentiating cerebral pilocytic astrocytoma and ganglioglioma BRAF V600E-mutant from wild type.** *Neuroradiology* 2020;62:71–80 CrossRef Medline
12. Rodriguez Gutierrez D, Awwad A, Meijer L, et al. **Metrics and textural features of MRI diffusion to improve classification of pediatric posterior fossa tumors.** *AJNR Am J Neuroradiol* 2014;35:1009–15 CrossRef Medline
13. Bull JG, Saunders DE, Clark CA. **Discrimination of paediatric brain tumours using apparent diffusion coefficient histograms.** *Eur Radiol* 2012;22:447–57 CrossRef Medline
14. Parmar C, Rios Velazquez E, Leijenaar R, et al. **Robust radiomics feature quantification using semiautomatic volumetric segmentation.** *PLoS One* 2014;9:e102107 CrossRef Medline
15. van Griethuysen JJ, Fedorov A, Parmar C, et al. **Computational radiomics system to decode the radiographic phenotype.** *Cancer Res* 2017;77:e104–07 CrossRef Medline
16. Ishi Y, Yamaguchi S, Yoshida M, et al. **Correlation between magnetic resonance imaging characteristics and BRAF alteration status in individuals with optic pathway/hypothalamic pilocytic astrocytomas.** *J Neuroradiol* 2021;48:266–270 CrossRef Medline
17. Wagner MW, Hainc N, Khalvati F, et al. **Radiomics of pediatric low-grade gliomas: toward a pretherapeutic differentiation of BRAF-mutated and BRAF-fused tumors.** *AJNR Am J Neuroradiol* 2021; 42:759–765 CrossRef Medline
18. Ryall S, Tabori U, Hawkins C. **Pediatric low-grade glioma in the era of molecular diagnostics.** *Acta Neuropathol Commun* 2020;8:30 CrossRef Medline
19. Lee S, Choi SH, Ryoo I, et al. **Evaluation of the microenvironmental heterogeneity in high-grade gliomas with IDH1/2 gene mutation using histogram analysis of diffusion-weighted imaging and dynamic-susceptibility contrast perfusion imaging.** *J Neurooncol* 2015;121:141–50 CrossRef Medline
20. Lee MK, Park JE, Jo Y, et al. **Advanced imaging parameters improve the prediction of diffuse lower-grade gliomas subtype, IDH mutant with no 1p19q codeletion: added value to the T2/FLAIR mismatch sign.** *Eur Radiol* 2020;30:844–54 CrossRef Medline
21. Koh DM, Collins DJ. **Diffusion-weighted MRI in the body: applications and challenges in oncology.** *AJR Am J Roentgenol* 2007;188:1622–35 CrossRef Medline
22. Guo AC, Cummings TJ, Dash RC, et al. **Lymphomas and high-grade astrocytomas: comparison of water diffusibility and histologic characteristics.** *Radiology* 2002;224:177–83 CrossRef Medline
23. Doskaliyev A, Yamasaki F, Ohtaki M, et al. **Lymphomas and glioblastomas: differences in the apparent diffusion coefficient evaluated with high b-value diffusion-weighted magnetic resonance imaging at 3T.** *Eur J Radiol* 2012;81:339–44 CrossRef Medline
24. Calli C, Kitis O, Yunten N, et al. **Perfusion and diffusion MR imaging in enhancing malignant cerebral tumors.** *Eur J Radiol* 2006;58:394–403 CrossRef Medline
25. Gihr G, Horvath-Rizea D, Hekeler E, et al. **Diffusion weighted imaging in high-grade gliomas: a histogram-based analysis of apparent diffusion coefficient profile.** *PLoS One* 2021;16:e0249878 CrossRef Medline
26. Aboian MS, Tong E, Solomon DA, et al. **Diffusion characteristics of pediatric diffuse midline gliomas with histone H3-K27M mutation using apparent diffusion coefficient histogram analysis.** *AJNR Am J Neuroradiol* 2019;40:1804–10 CrossRef Medline
27. Kang Y, Choi SH, Kim YJ, et al. **Gliomas: histogram analysis of apparent diffusion coefficient maps with standard- or high-b-value diffusion-weighted MR imaging—correlation with tumor grade.** *Radiology* 2011;261:882–90 CrossRef Medline
28. Lobon-Iglesias MJ, Laurendeau I, Guerrini-Rousseau L, et al. **NF1-like optic pathway gliomas in children: clinical and molecular characterization of this specific presentation.** *Neurooncol Adv* 2020;2:i98–106 CrossRef Medline
29. Matsuoka A, Minato M, Harada M, et al. **Comparison of 3.0-and 1.5-Tesla diffusion-weighted imaging in the visibility of breast cancer.** *Radiat Med* 2008;26:15–20 CrossRef Medline
30. Saremi F, Jalili M, Sefidbakht S, et al. **Diffusion-weighted imaging of the abdomen at 3 T: image quality comparison with 1.5-T magnet using 3 different imaging sequences.** *J Comput Assist Tomogr* 2011;35:317–25 CrossRef
31. Sasaki M, Yamada K, Watanabe Y, et al; Acute Stroke Imaging Standardization Group-Japan (ASIST-Japan) Investigators. **Variability in absolute apparent diffusion coefficient values across different platforms may be substantial: a multivendor, multi-institutional comparison study.** *Radiology* 2008;249:624–30 CrossRef Medline
32. Tsujita N, Kai N, Fujita Y, et al. **Interimager variability in ADC measurement of the human brain.** *Magn Reson Med Sci* 2014;13:81–87 CrossRef Medline
33. Wu CC, Jain R, Radmanesh A, et al. **Predicting genotype and survival in glioma using standard clinical MR imaging apparent diffusion coefficient images: a pilot study from the Cancer Genome Atlas.** *AJNR Am J Neuroradiol* 2018;39:1814–20 CrossRef Medline
34. Harreld JH, Hwang SN, Qaddoumi I, et al. **Relative ADC and location differ between posterior fossa pilocytic astrocytomas with and without gangliocytic differentiation.** *AJNR Am J Neuroradiol* 2016;37:2370–75 CrossRef Medline
35. McDonald CR, Delfanti RL, Krishnan AP, et al. **Restriction spectrum imaging predicts response to bevacizumab in patients with high-grade glioma.** *Neuro Oncol* 2016;18:1579–90 CrossRef Medline
36. Rodriguez Gutierrez D, Manita M, Jaspan T, et al. **Serial MR diffusion to predict treatment response in high-grade pediatric brain tumors: a comparison of regional and voxel-based diffusion change metrics.** *Neuro Oncol* 2013;15:981–89 CrossRef Medline
37. Poussaint TY, Vajapeyam S, Ricci KI, et al. **Apparent diffusion coefficient histogram metrics correlate with survival in diffuse intrinsic pontine glioma: a report from the Pediatric Brain Tumor Consortium.** *Neuro Oncol* 2016;18:725–34 CrossRef Medline